Atmos. Chem. Phys. Discuss., 12, 14875–14926, 2012
www.atmos-chem-phys-discuss.net/12/14875/2012/
doi:10.5194/acpd-12-14875-2012


Atmospheric Chemistry and Physics Discussions



# On the origin of subvisible cirrus clouds in the tropical upper troposphere

**M. Reverdy**[1], **V. Noel**[2], **H. Chepfer**[3], **and B. Legras**[2]

[1]CNES, Laboratoire de Meteorologie Dynamique (IPSL), UMR8539, Ecole Polytechnique, 91128 Palaiseau, France
[2]CNRS, Laboratoire de Meteorologie Dynamique (IPSL), UMR8539, Ecole Polytechnique, 91128 Palaiseau, France
[3]UPMC, Laboratoire de Meteorologie Dynamique (IPSL), UMR8539, Ecole Polytechnique, 91128 Palaiseau, France

Received: 26 April 2012 – Accepted: 24 May 2012 – Published: 12 June 2012

Correspondence to: M. Reverdy (mathieu.reverdy@lmd.polytechnique.fr)

Published by Copernicus Publications on behalf of the European Geosciences Union.







## Abstract

Spaceborne lidar observations have recently revealed a previously undetected significant population of SubVisible Cirrus (SVC). We show them to be colder than −74 °C, with an optical depth below 0.0015 on average. The formation and persistence over time of this new cloud population could be related to several atmospheric phenomena. In this paper, we investigate the importance of external processes in the creation of this cloud population, vs. the traditional ice cloud formation theory through convection. The importance of three scenarios in the formation of the global SVC population is investigated through different approaches that include comparisons with data imaging from several spaceborne instruments and back-trajectories that document the history and behavior of air masses leading to a point in time and space where subvisible cirrus were detected. In order simplify the study of cloud formation processes, we singled out SVC with coherent temperature histories (mean variance lower than 4 K) according to back-trajectories along 5, 10 or 15 days (respectively 58, 25 and 11 % of SVC). Our results suggest that external processes, including local increases in liquid and hygroscopic aerosol concentration (either through biomass burning or volcanic injection forming sulfate-based aerosols in the troposphere or the stratosphere) have no noticeable short-term or mid-term impact on the SVC population. On the other hand, we find that ∼ 60 % of air masses interacted with convective activity in the days before they led to cloud formation and detection, which correspond to 37 to 65 % of SVC. These results put forward the important influence of classical cloud formation processes compared to external influences in forming SVC. They support the view that the SVC population observed by CALIOP is an extension of the general upper tropospheric ice clouds population with its extreme thinness as its only differentiating factor.






ACPD
12, 14875–14926, 2012



## 1 Introduction

Subvisible cirrus (SVC) are optically thin ice clouds with optical depths below 0.03 mostly found in the tropical upper troposphere. Their existence has been known for several decades thanks to in-situ measurements from airborne probes (e.g., Heymsfield, 1986) and ground-based observations (Sassen and Cho, 1992). These studies were able to document the composition of some SVC (e.g., Davis et al., 2007, 2010; Lawson et al., 2008), but are hard to generalize globally. Limb observations from spaceborne instruments such as SAGE-II (Wang et al., 1994) led to important insights about these clouds, but are generally limited by a poor spatial resolution.

The role of SVC in several upper tropospheric processes is still unclear. Due to their optical transparency and cold temperatures, high tropospheric ice clouds present a limited albedo effect but some greenhouse effect, by which they modulate the global radiative budget. Most importantly, their mechanisms of formation and evolution are not well understood. This has serious implications for atmospheric physics: SVC in the Tropical Tropopause Layer (TTL, Fueglistaler et al., 2009) are often associated with the dehydration of air before it enters the stratosphere. Our poor understanding of how they interact with water vapour, which may lead to persistent supersaturation within SVC (Peter et al., 2005) means their influence as regulators at the troposphere–stratosphere interface cannot be correctly reproduced by models. This leads, among other things, to high uncertainties in the modeling of stratospheric water vapor evolution, which has consequences for climate prediction (Solomon et al., 2010).

Recent advances in signal analysis, and the availability of spaceborne active remote sensing observations, have allowed the global-scale detection of upper tropospheric layers with extremely small optical depths (down to 0.001), far thinner optically than what was previously possible using satellite observations. Most notably, observations from the Cloud-Aerosol Lidar with Orthogonal Polarization (CALIOP, Winker et al., 2009) have for the first time documented the large spatial and temporal cover of SVC (e.g., Sassen et al., 2009; Martins et al., 2011). Using the same observations,





ACPD
12, 14875–14926, 2012



Pan and Munchak (2011) found such clouds are frequently close to the TTL and extend sometimes horizontally over several thousand kilometers. The increase in the estimated overall cover of optically very thin clouds following these discoveries means estimates of their radiative impact had to be revised (Haladay and Stephens, 2009; Yang et al., 2010; Dupont et al., 2010).

In the wake of the documentation of this large number of optically thin particle layers, and the uncertainty surrounding their formation processes, it is important to address the question of whether they should be considered as an extension of the generic high troposphere cloud population (and thus follow traditional cloud formation theories, including convection and in-situ nucleation) with small optical depths as their only specificity, or whether their formation and composition are significantly affected by external processes (in which case they constitute a population with a specific composition and qualitatively different intrinsic properties that needs to be addressed separately from the generic cloud population). The answer to this question would shed light on the role played by SVC in atmospheric processes. For instance, the inclusion of organic aerosols, sulfate or nitric acid within nucleating ice crystals would have serious implications for the ability of SVC to dehydrate the upper troposphere, as it has been shown to severely limit water vapor deposition (Kramer et al., 2006; Murray, 2008; Grenier and Blanchet, 2010), and could be the cause leading to persisting supersaturation in clear air or around SVC (Kramer et al., 2009).

To address this question, in the present article we first document the properties of cloud layers identified as SVC in the Tropics from CALIOP observations (Sect. 2). We then document the history of air masses that led to the formation of these layers using back-trajectories (Sects. 3 and 4). By merging these results with complementary satellite data, we investigate the possibility that two atmospheric phenomena (aerosol injection from eruptions and biomass burning, nucleation of trihydrate crystals through $HNO_3$ deposition) have a detectable impact on the formation of these layers (Sect. 5). In the same section, we confront these results with the frequency of convection events





ACPD
12, 14875–14926, 2012



in the recent history of air masses leading to SVC formation, obtained through a similar method.

## 2 SVC observations from CALIOP

CALIOP is located on the CALIPSO satellite (Cloud-Aerosol Lidar and Infrared Pathfinder Satellite Observation), part of the A-Train, which follows a nearly sun-synchronous orbit that crosses the equator twice per day, at 01:30 and 13:30 local time. CALIOP measures range-resolved vertical profiles of elastic backscatter at 532 and 1064 nm, which document the vertical distribution of atmospheric composition. By applying a cloud detection algorithm dedicated to optically thin layers over more than 2 yr of CALIOP observations (June 2006–December 2008), we have generated a dataset of cloud base and top along the CALIPSO track with a 5 km resolution. The algorithm and dataset are documented at length in Martins et al. (2011). In addition, the optical depth $\tau$ of each cloud was retrieved by layer-integrating attenuated backscatter profiles from CALIOP level 1 data, following Platt et al. (2002) as

$$\tau = \frac{1}{2\eta}\ln(1 - 2S\eta\gamma')$$

where $\gamma'$ is the total attenuated backscatter coefficient at 532 nm integrated over the cloud layer, $S$ is the lidar ratio and $\eta$ is the multiple scattering coefficient. As in previous works (Noel et al., 2007; Winker et al., 2009), we assumed constant values $S = 25$ sr and $\eta = 0.7$. The impact of these choices on the retrieved optical depth is discussed in Martins et al. (2011). The obtained dataset, called SEL2 for Subvisible-Enhanced Level 2 is available for studies focusing on subvisible cirrus at http://climserv.ipsl.polytechnique.fr/sel2.html.

CALIOP observations can be exploited to retrieve indications about the microphysical properties of particles within the SVC. In the polarization-sensitive 532 nm channel,





ACPD
12, 14875–14926, 2012



the ratio of backscattered light in the perpendicular and parallel planes of polarization defines the depolarization ratio (Sassen, 1991). It depends on particle shape and is routinely used in cloud observations to discriminate liquid water droplets (spherical) from ice crystals (non-spherical). The ratio of backscattered light in the 1064 and 532 nm channels defines the color ratio, which provides information about particle size (Vaughan et al., 2010). Particulate backscatter was calculated by removing the molecular contribution from the CALIOP total attenuated backscatter, using the same approximation as in Martins et al. (2011). The molecular contribution had to be removed as it can be significant in optically thin features such as SVC. Section 4 focuses on these ratios within SVC.

We identified subvisible cirrus clouds in the SEL2 database by requiring (1) layer optical depths $\tau$ below 0.03, following the widely used convention from Sassen and Cho (1992), and (2) layer temperatures colder than −40 °C (to ensure only the ice phase was present), using GEOS-5 temperatures included in CALIOP level 1 data. To limit the inclusion of spurious detection from signal noise, we restricted our analysis to SVC extending over at least 200 km along-track, or 40 consecutive 5 km-wide profiles. Vertically contiguous layers distant horizontally by less than 10 km (spanning 2 profiles) were considered to be part of the same cloud. Since a large majority of cirrus clouds lie in the Tropics (30° S–30° N) according to CALIOP studies (e.g., Sassen et al., 2008), we have restricted our SVC analysis to this region. Figure 1a shows an example of SVC layers detected in a single CALIPSO overpass over the Tropics on 6 August 2007 (orbit T07-03-58). The filtering described above identified two SVC in this overpass between 15 and 17 km of altitude (Fig. 1b), both with temperatures near −75 °C (198 K) and optical depths near 0.004.

We analyzed SVC during the boreal summer (JJA) and winter (DJF), the two periods with the largest proportion of tropical cirrus cover (Massie et al., 2010). Between 30° S and 30° N, over the 2006–2008 period, 2810 SVC were detected in JJA and 4039 in DJF. SVC temperatures are between 185 and 215 K (Fig. 2, row 1) with maximum occurrence around 195 K, and are on average 5 K warmer in JJA. In both seasons,





ACPD
12, 14875–14926, 2012



SVC are 200 to 1200 m thick (row 2), and optically extremely thin (row 3): almost all of them exhibit $\tau < 0.015$, making them Ultra Thin Tropopause Clouds (Peter et al., 2003). These clouds are most frequently a few hundred kilometers wide, but can reach several thousand kilometers on occasion (row 4), which explains why their average horizontal extent is close to 500 km. While the temperature distributions are not Gaussian with a tail towards warm temperatures, the distributions of thickness are close to Gaussian both in geometrical height and optical depth. Relating these properties to specific mechanisms is not straightforward, but these observations will have to be accounted by models of SVC generation. The horizontal extent exhibits a very skewed distribution with a long tail towards large values. This suggests a non diffusive dispersion with large dispersion being induced by shear and filamentary structures.

The geographic distribution of SVC in a 10° × 10° grid (Fig. 3) over the tropical region (±30°) shows most are located between 10° S and 10° N along the Intertropical Convergence Zone (ITCZ), with fewer SVC closer to mid-latitudes. Maxima are in regions of deep convection (Central America, Africa, Asia and Western Pacific), identified by the contour lines showing minima of outgoing longwave flux as observed by CERES over the same periods. In JJA, maxima are over the Eastern region of Asian Monsoon and the Arabian Sea. In DJF, SVC are much more numerous and maxima are over Western Pacific, Central Africa and the Amazon Basin. Cloud fractions are low over Atlantic and Eastern Pacific Oceans in both seasons. This geographic distribution is consistent with Massie et al. (2010) and Martins et al. (2011).

## 3 Back-trajectories

### 3.1 Model setup and initialization

Back-trajectories use time-resolved wind fields from meteorological analysis or reanalysis to document the three dimensional time itinerary followed by air masses. By using additional fields, one can retrieve atmospheric properties (e.g. temperature)





ACPD
12, 14875–14926, 2012



along the trajectory. We resolved back-trajectories with the TRACZILLA model (James and Legras, 2009), a modified version of the Lagrangian trajectory model FLEXPART (Stohl et al., 2005). By contrast with FLEXPART, TRACZILLA provides an advection scheme that discards the intermediate terrain following coordinate system, and performs a direct vertical interpolation of winds, linear in log-pressure, from hybrid levels (Pisso and Legras, 2008). Its reverse integration of trajectories uses wind fields from combined re-analysis and 3-h forecasts from the ECMWF (European Center of Medium range Weather Forecast) ERA-Interim dataset (Dee et al., 2011), on a 1° longitude-latitude grid and 60 vertical hybrid levels (Legras et al., 2005).

For each SVC detected by CALIOP and meeting the criteria from Sect. 2, a Cartesian domain was defined bounded by the cloud beginning and end coordinates in the corresponding CALIOP orbit. This domain was then discretized in 1° × 1° boxes. In the regions under study, this means dividing each SVC in roughly 100-km sections along-track. The TRACZILLA model released particles in each box center at the mean SVC altitude within the box, and followed their back-trajectories 15 days prior with a 1-h sampling (360 points). Thus, multiple back-trajectories were calculated for each SVC according to its horizontal extent. On average, ten back-trajectories were launched per SVC, although this number climbed over 100 for clouds extending over several thousand kilometers.

Back-trajectories form different patterns depending on their starting point. Figure 4 displays three representative examples of 15-days back-trajectories in JJA, initialized at the time and location of SVC identified by dots. For the SVC detected over South Asia on 11 June 2007 (red), back-trajectories follow a round shape that is typical for initialization over this region. By contrast, an SVC detected over Central America on 31 July 2007 (blue) leads to straight back-trajectories that do not deviate much from the SVC latitude. This is typical behavior for back-trajectories initialized near the equator, which typically extend over much longer ranges. A last back-trajectory, associated with an SVC observed over Central America on 29 June 2006, shows a more complex





ACPD
12, 14875–14926, 2012



shape (green). In our results, back-trajectories initialized far from the equator generally tend to spread out more.

### 3.2 Temperature history coherence

Back-trajectories initialized in the same vicinity tend to separate over time due to the chaotic properties of advection in a time-varying flow. For instance, the green back-trajectories in Fig. 4 initially originate from nearby sections of the same SVC, but drift apart significantly as time goes back. Due to natural air mass dispersion, the distance between them can reach several degrees, and they eventually spread over the whole tropical belt (Tzella and Legras, 2011). As back-trajectories drift apart, the histories of air masses leading to the observed SVC start to diverge, mixing becomes significant and it gets harder to identify mechanisms responsible for cloud formation. In order to avoid the complexities linked to the tracking of air masses mixing, we elected to constrain our study to SVC coming from a single air mass. Since temperature is a major factor of ice nucleation processes, we used its variance history to quantify back-trajectories dispersion. For an SVC with $n$ back-trajectories, we computed for each of the 360 time points the temperature variance among the $n$ back-trajectories. The resulting temperature variance time series was then averaged over 5, 10 and 15-days windows back in time. A small temperature variance means that all back-trajectories can be considered to share a common history during the time window. Conversely, large temperature variances are a sign of dispersion, i.e. the histories of the $n$ back-trajectories diverge significantly.

Figure 5a shows the distribution of temperature variances among 15 days back-trajectories for all SVCs. Back-trajectories with temperature variance below 4 K were classified as "coherent 1" (C1), temperature variance between 4 and 8 K as "coherent 2" (C2) and temperature variance above 8 K as "divergent" (D). Figure 5b, c show examples of temperature histories and how the associated SVC was classified according to the criterion explained above. Figure 5b shows a case with roughly constant temperature (around −75 °C) for all back-trajectories. This SVC was categorized as C1 at





ACPD
12, 14875–14926, 2012



5, 10 and 15 days back in time. Figure 5c shows a case in which the temperature decreases significantly during the first 5 days back in time, but temperature variance stays low. As times goes back, temperature variance increases, a sign of history divergence among back-trajectories. The associated SVC was characterized as C1 at 5 days back in time, and D at 10 days and 15 days.

We studied SVC temperature history coherence in 5 geographical areas described in Table 1 and shown in Fig. 4, similar to those used by Riihimaki and McFarlane (2010). Asia and Africa regions are truncated to accommodate the Asian Monsoon Anticyclone region (AMA), a special case due to its specific meteorology. Numbers of SVC classified as C1, C2 or D based on their temperature history over 15 days are presented by region in Table 2 for JJA (top) and DJF (bottom). In Fig. 6 Asia, Africa and Central America stand out again as SVC hotspots (as in Fig. 3). Temperature coherence does not change a lot between winter and summer, except over the AMA region where it almost vanishes during winter. Over 10 days (not shown), the number of C1 SVC more than doubles ($\sim$25 %) while the number of C2 SVC increases slightly (to $\sim$12 %). Over 5 days, the number of C1 SVC more than doubles again ($\sim$58 %). We understand the C2 state as a transitory phase between C1 and D categories.

The rest of the paper will focus on C1 SVC with the most coherent temperature history before cloud formation, based on the assumption that it should be easier to identify mechanisms responsible for their formation. 15-days temperature histories are used throughout except for the convection study (Sect. 5.3) where 5-days histories are used due to geographical constraints.

## 4 SVC with coherent temperature histories

### 4.1 Geographical distribution and properties of C1 SVC

Figure 7 shows the geographical distribution of C1 SVC. In DJF, there are noticeably more SVC over the Gulf of Guinea and Africa ($\sim$6 %) and less elsewhere. In JJA, SVC





ACPD
12, 14875–14926, 2012



are more scattered, with disputable hotspots over the Western Pacific, Central America and West Africa. Geographic distributions of C1 SVC do not necessarily match those of the general SVC population (Fig. 3). Table 3 describes how C1 SVC fall in five temperature ranges. Almost half of C1 SVC (45.4 %) are in the middle 191–195 K range, 26.5 % in the 188–191 K range and 17.5 % in the 195–205 K range. The remaining small number of C1 SVC (10.6 %) are either very cold (183–188 K) or very "warm" (205–215 K). 55.4 % of C1 SVC are detected in DJF and 44.6 % in JJA, which is close to the distribution of the entire SVC population (Sect. 2). According to the Kolmogorov-Smirnov test at a 5 % significance level, C1 SVC are colder, optically and geometrically thinner than the general SVC population.

We calculated the cloud depolarization and color ratios (Sect. 2) for each SVC averaged over its vertical range and horizontal sections used as starting points for back-trajectories (Sect. 3.1). Distributions of depolarization ratio vs. temperature (Fig. 8, top), and of depolarization vs. color ratio (Fig. 8, bottom) suggest groups with distinct optical properties. A large group shows large depolarization (0.3–0.5), temperatures near 193 K and color ratios close to 1 (88.6 % of SVC). These properties are consistent with large, non-spherical particles such as ice crystals from typical upper tropospheric clouds (Sassen and Benson, 2001). A much smaller group at temperatures near 205 K shows near-zero depolarization ratio and small color ratios (below 0.4), typical of near-spherical small particles (8 % of SVC). Almost all layers belonging to this second group were observed in the low stratosphere during JJA 2006, and were identified by Carn et al. (2007) as sulfate aerosols produced after injection of $SO_2$ in the stratosphere by the eruption of the Soufrière Hills volcano (Montserrat) on 20 May 2006. These layers extended over several thousand kilometers and dispersed slowly while traveling around the globe for several weeks. We will not consider them as clouds here, as they are purely stratospheric, but will discuss their potential impact on the SVC population in Sect. 5.2.





ACPD
12, 14875–14926, 2012



### 4.2 Histories of air masses leading to C1 SVC

Here we focus on Africa in DJF and the Pacific in JJA, areas which contain the largest number of C1 SVC detections. Figure 9 shows these detections between 2006 and 2008 (top row), and the spatial distribution of associated 5, 10 and 15-days back-trajectories. For DJF SVC over Africa (left column), most air masses originate from the same area and stay there, with a few coming from Asia and America. Moving back in time from 5 to 15 days, maximum densities gradually shift away from the gulf of Guinea toward the Somali Basin. For JJA SVC observed over Pacific (right column), most air masses originate from the same vicinity, but as time goes back maxima shift to the East and to Central America. At 15 days, the Atlantic becomes a non-negligible source for air leading to Pacific SVC.

Figure 10 shows histograms of total length travelled by back-trajectories versus the distance reached at their furthest point away from the SVC of origin, for back-trajectories classified as C1 over 15, 10 and 5 days in JJA Pacific and DJF Africa. The total length exhibits similar range over both regions (up to $\sim$30 000 km), but distributions differ. Over the Pacific (left column), long trajectories (total lengths > 10 000 km, up to 22 000 km) are as common as short ones, and a minority of extremely long paths reach 35 000 km. By contrast, over Africa (right column), short trajectories (5000–12 000 km) clearly dominate. This is consistent with Fig. 9, which shows longer trajectories being more prevalent over Pacific than over Africa. Over 15 days (top row), 3 groups can be identified over both regions:

1. short total length (< 12 000 km) and much smaller reach. These paths are roughly circular, and do not stray far away from the area of SVC detection (similar to the red path in Fig. 4).

2. roughly equal total length and reach, close to the identity line (12 000–20 000 km). These paths are roughly straight (similar to the blue path in Fig. 4).





ACPD
12, 14875–14926, 2012



3. long total length (> 20 000 km) and relatively short reach. These trajectories have complicated shapes which are neither circular nor straight.

Shorter time periods (rows 2 and 3) mean back-trajectories travel over shorter distances and have shorter total lengths. As a consequence they are less likely to evolve complicated shapes and the distributions aggregate around the identity line in both regions. Curved trajectories (reach ≪ total length) still appear in DJF Africa over 10 days (right column). This suggests that trajectories need at least 10 days to evolve a circular shape.

## 5 Three candidate processes for SVC formation

This section investigates the possibility that three atmospheric processes help create the population of C1 SVC identified in Sect. 4: inclusion of nitric acid, nucleation of ice crystals on liquid or solid aerosols, and convection.

### 5.1 Inclusion of nitric acid

The formation of Nitric Acid Trihydrate crystals (NAT) by mixing of water vapor and $HNO_3$ near 195 K has been observed in the polar stratosphere for more than a decade (Voigt et al., 2000). These crystals can be distinguished from pure ice crystals by their specific optical signatures (e.g., Noel et al., 2008). The possibility of NAT crystals forming in the similarly cold TTL has been suggested by in-situ observations in the subtropics (Popp et al., 2004; Voigt et al., 2007, 2008). The detection of such particles in CALIOP observations is controversial since it is unclear whether the extremely low TTL concentrations of $HNO_3$ can lead to NAT concentrations measurable from space (Poole et al., 2009; Noel and Chepfer, 2009).

As discussed in Chepfer and Noel (2009), such particles would produce intermediate values of depolarization ratio (0.05–0.25) and color ratio (0.4–0.6). Such values make a faint apparition in our dataset (Fig. 8), at temperatures near 200 K (3.4 % of C1 SVC).





ACPD
12, 14875–14926, 2012



Remote sensing observations alone cannot ascertain the exact nature of the particles under study, but analyzing the temperature history of the air masses leading to SVC formation can provide useful circumstantial evidence to support or infirm the possibility of $HNO_3$ inclusion. For instance, the formation of NAT crystals requires sustained $HNO_3$ supersaturation for long periods (Voigt et al., 2008), as their nucleation process is considerably slower than ice.

Figure 11a shows the total trajectory length vs. the reach away from SVC over 15 days associated with C1 SVC with depolarization ratios in the 0.05–0.25 range (106 SVC). 30 % of trajectories are nearly straight with large total lengths and reaches (10 000–20 000 km). 37 % of them deviate from straightness, with total length below 15 000 km and reach below 8000 km. Temperature distribution (Fig. 11b, right) shows a small, cold group (190–197 K, 22 %), a tall narrow group in the 197–203 K range (34 %) and a warm group (205–210 K, 28 %). This suggests that a relatively large number of C1 SVC with depolarization ratios similar to NAT crystals stem from air masses that travelled along a relatively straight trajectory at stable temperatures colder than 197 K (56 % of trajectories) over long periods (up to two weeks). Such conditions would physically allow the nucleation of NAT crystals given adequate $HNO_3$ levels. In any case, it should be kept in mind that only 3.4 % of C1 SVC are concerned.

### 5.2 Local increase in aerosol concentration

Background aerosols are a potent source of SVC formation (Thomas et al., 2002). There are many possible pathways for ice nucleation from aerosols, whose local importance depends strongly on temperature, mixing ratios of participating chemical species, aerosol concentrations and size distribution (Lohmann and Diehl, 2006). In the TTL, the possible pathways are somewhat constrained but remain numerous. Background sulfuric acid particles grow by absorbing water vapor at any relative humidity with respect to water, and can subsist as liquid droplets for a long time. Such liquid sulfate aerosols (Jensen et al., 1996) and organic aerosols (Karcher and Koop, 2005) brought from the surface by convection can freeze either homogeneously or heterogeneously (through





ACPD
12, 14875–14926, 2012



interaction with solid aerosols), leading to ice nucleation. Recent research suggests that dry ammonium sulfate particles are efficient ice nuclei (Jensen et al., 2010), but other aerosols such as mineral dust and organic carbon (Karcher, 2002) can also play this role. Due to this complexity, the dominant formation processes of in-situ ice clouds in the TTL has still not been asserted with certainty (Froyd et al., 2010), although the importance of anthropogenic emissions seems notable (Weigel et al., 2011).

Because it would be too complex to identify the ice nucleation pathway of each SVC in our dataset, we tried instead to detect a correlation between SVC cover and local increase in the atmospheric concentrations of certain species due to specific events that provide sources of ice nuclei. As a first instance, we investigate increases in concentration of sulfate-based aerosols and dust that follow volcanic degassing and eruptions (Lohmann et al., 2003; Bingemer et al., 2012). Were such aerosols to play a significant role in the formation of the observed SVC population, an increase in sulfate levels would lead to a corresponding increase in SVC cloud cover.

Three significant eruptions happened in the tropical band ($\pm 30^{\circ}$) during the 2006–2008 period that we study here. The Tavurvur ($4^{\circ}$ S) erupted on 7 October 2006 and led to a direct injection of chemical species in the TTL and lower stratosphere, although its plume was rapidly advected to higher latitudes (well-documented in Vernier et al., 2011a). The Nyiragongo in DR Congo erupted through November and December 2006. Figure 12 maps the total column of $SO_2$ concentration ($0.125 \times 0.125^{\circ}$) on 27 November 2006 (top), a few days in the eruption, using the OMSO2G product from the Ozone Monitoring Instrument (OMI), on board the Aura satellite (part of the A-Train). Important local enhancements of $SO_2$ are obvious over Africa spreading east. Three days later (Fig. 12, bottom), the plume is still strong but has moved towards the AMA. A last, smaller eruption happened in Hawaii in June 2006. Its plume stayed over the Pacific a long time, moving west before dissipating over Asia. These last two eruptions failed to inject chemical species directly in the UTLS (Yang et al., 2007) but through interaction with convection could lead to significant enhancement near the TTL. The three eruptions severely impacted the horizontal distribution of $SO_2$. Other eruptions





ACPD
12, 14875–14926, 2012



during this period had low explosivity index or happened outside of the tropical band (Vernier et al., 2011b), and thus would have smaller effects on tropical SVC. To study how the $SO_2$ injected in the troposphere by those three eruptions impacts SVC formation, we describe the total number of C1 SVC observed over five regions and seasons in Table 4. Bold indicates when a plume from either eruption reached the region (DJF 2006–2007 and JJA 2006), and months of eruption are underlined. Volcanic plumes led to significant local $SO_2$ enhancements over long distances in four areas: Africa, Asia, AMA and Pacific. After the Nyiragongo eruption (DJF 2006–2007), the number of SVC detections does not change significantly compared to DJF 2007–2008 (no eruption). The same absence of impact is found for the Tavurvur and Hawaii eruptions (comparing 2006 and 2007). Figure 13 shows how the SVC cloud fraction evolves with time in the Tropics (±30°, blue line) in the SEL2 dataset. The period through June to October 2006, including the Tavurvur and Hawaii eruptions (and the Soufriére Hills eruption, studied below), shows no increase in cloud fraction. The increase from mid-october to mid-december 2006 began before the Nyiragongo eruption, so it cannot be due to an instantaneous increase in tropospheric $SO_2$. It could however be explained by a delayed increase once the volcanic emissions had spread over the convection band and interacted with enough convective events to bring a significant amount of particles in the upper troposphere. This increase is however comparable to a similar one in May 2007 that happened during an eruption-free period. Unrelated to volcanic eruptions, Vernier et al. (2011c) used CALIOP observations to identify a seasonal enhancement of the background aerosol concentration in the upper troposphere (13–18 km altitude range) every year between June and August in the area under the influence of the Asian Monsoon (15–45° N, 5–105° E). This area is part of the tropical band we study (±30°). Figure 13 shows the SVC cloud fraction in this area (green line) fluctuates considerably (probably due to the smaller sample size), but is on average equal to the one over the whole tropical band (1.6 % for both). It is indeed higher than average from June to August 2006, a pattern that however does not repeat in 2007 or 2008.





ACPD
12, 14875–14926, 2012



Such a seasonal influence would however be difficult to separate from the effects of the convective activity cycle itself.

As mentioned in Sect. 4.1, the Soufrière Hills stratovolcano (16.7° N, 62.2° W) erupted little before the first CALIOP observations in May 2006, injecting volcanic ash and $SO_2$ at least as high as 18 km. The resulting layer of sulfate-based aerosols travelled in the stratosphere for several weeks in the 15–30° N band, and was clearly visible in CALIOP observations at altitudes between 19 and 21 km until mid-July (Carn et al., 2007). This eruption arguably had the biggest influence on the composition of the lower stratosphere during the studied period (Vernier et al., 2011a). Figure 14 (top) shows the backscatter coefficient observed by CALIOP as a Hovmöller diagram function of longitude and time between May and December 2006, averaged in the latitude and altitude ranges defined above. In June, the location of the stratospheric layer is clearly identified by relatively high backscatter levels ($\sim 2 \times 10^{-4}$ km$^{-1}$ sr$^{-1}$) above the weaker stratospheric background backscatter (1 to $1.3 \times 10^{-4}$ km$^{-1}$ sr$^{-1}$). Its westward trajectory can be tracked fairly well, circling the globe ~ 3 times until mid-September, at which point it had merged with background concentrations throughout the whole tropical band. Meanwhile, the average backscatter at the same altitude levels (Fig. 14, bottom), which can be understood as a proxy for the amount of aerosol loading in the lower stratosphere, stays relatively high until it goes back to pre-eruption levels in November, at which point the sulfate-based aerosols have left the monitored band by being most probably lofted to higher altitudes. Analyzing the cloud cover of tropospheric SVC in the same latitude band as a function of longitude and time (not shown) over the June–September period shows no instantaneous correlation with the stratospheric layer trajectory. Similarly, the only increase in average tropical SVC cloud fraction during the same timeframe (Fig. 13, blue line) happens between mid-October and mid-December (+30 % at its peak). Relating this pattern to any increase in high troposphere ice nuclei concentrations following the sedimentation of the stratospheric sulfate-based aerosols through the TTL is difficult given the Soufriére Hills eruption was modest in terms of stratospheric $SO_2$ loading (0.1 Tg, Prata et al., 2007).





ACPD
12, 14875–14926, 2012



Finally, we took a brief look at a biomass burning event (as in Spichtinger et al., 2001). Such events are frequent over Africa and Madagascar, and produce hygroscopic organic aerosols that can act as ice nuclei (Petters et al., 2009). To investigate the importance of such aerosols on SVC formation, we used observations of the daily total column of $NO_2$ concentration from OMI (OMNO2G product, same resolution as OMSO2G) as a proxy for biomass burning intensity. Figure 15 presents a map of average $NO_2$ concentration for February 2007 as observed by OMI. Conducting a study of SVC detections against $NO_2$ activity (similar to what was done with Table 4) and investigating the correlation between time series of SVC detection and $NO_2$ concentration (not shown here) led to the same results as with $SO_2$: no noticeable correlation. In fact, SVC cloud fractions are similar over Pacific and Africa, where $NO_2$ concentrations are respectively low and high.

### 5.3 Convective activity

Detrainment from cloud systems generated by deep convection is important for SVC formation (see e.g., Jensen et al., 1996). For instance, tropical cumulonimbus can generate extensive cirrus outflow anvils from which larger crystals precipitate, leaving behind optically thin layers of small ice crystals. Isolated ice clouds can also form in-situ from humid air brought to high altitudes by convection and lofted above 15 km towards and across the cold point of the tropical tropopause by the mean clear air ascent (Fueglistaler et al., 2009).

Here we investigate whether C1 SVC can be linked to convective systems, identified as cold areas in maps of brightness temperature (BT) indicative of optically thick high altitude clouds (Arnaud et al., 1992), against the warm background of surface emissions. We used the ISCCP DX product (Rossow and Schiffer 1991; Stubenrauch et al., 1999) that contains a BT map every 3 h at 30 km horizontal resolution derived from METEOSAT infrared images. Since it covers a limited geographic area (60° W–60° E including Africa), we only considered the first 5 days of each back-trajectory, as over longer periods they often leave the domain. We extracted BT 150 km around each point





ACPD
12, 14875–14926, 2012



along each back-trajectory of each C1 SVC from the ISCCP map closest in time to the point (less than 1.5 h apart). We compared the coldest BT in this area with the temperature retrieved at the back-trajectory point altitude, estimated by TRACZILLA from the ECMWF input field. When both temperatures are cold, the air mass tracked by the back-trajectory travelled near the top of a high-altitude convective system. As an example, Fig. 16 shows brightness temperatures composited from 40 ISCCP maps covering 5-days trajectories back-propagating east from a SVC observed over the Atlantic on 13 June 2006. Most of the BT are warmer than 280 K (red) and denote clear-sky conditions. During the same period, the air masses tracked by the back-trajectories stay colder than 200 K (Fig. 17, red). This means that the air mass often travelled high above low-level clouds or the surface. Cold BT (180–200 K) appear 80–100 h before SVC detection (Fig. 17, black), in the 5° W–10° E area (blue in Fig. 16, near day 4), and indicate intersections with high-level convective systems. The difference between BT and back-trajectory temperature is less than 20 K in that period and area, symptomatic of an intersection with a high-altitude cloud system.

We analyzed in the same manner ∼500 back-trajectories for the 57 SVC detected over Africa during JJA 2006. These back-trajectories always stayed colder than 215 K, meaning all the tracked air masses travelled high in the upper troposphere over the five days preceding SVC formation. By comparison, surrounding BT are very warm most of the time (close to ground temperature), indicating that air masses mostly travel above areas in clear-sky conditions. For each trajectory, we identified where its temperature got closest to its surrounding BT. Figure 18 shows the distribution of the minimum temperature difference across all trajectories. In 48 % of those, both temperatures get less than 20 K apart somewhere along the path (less than 10 K apart in 28 %), meaning that almost half of the air masses had a close encounter with the top of an optically thick high-altitude cloud system (∼220 K) less than five days before SVC formation. In that period, those trajectories generally spend less than 24 cumulated hours over convective systems and mostly travel over clear-sky areas. 65 % of SVC are related to at least one back-trajectory crossing a convective system; in 37 % of SVC this is true for





ACPD
12, 14875–14926, 2012



all back-trajectories. Air masses spending more than 24 h above convective systems over the 5 days exist but are rare (less than 10 % of trajectories). On the other hand, 34 % of back-trajectories always stay more than 40 K away than their surrounding BT and travelled only over low-level clouds or the surface. Note that cloud top temperatures retrieved through thermal imagery analysis have a warm bias of at least several K, as the ice-based translucent top of convective systems lets warm emissions shine through from lower parts of the cloud (Sherwood et al., 2004). Actual cloud top temperatures are thus probably colder than the reported BT and the numbers reported here are probably underestimates. The points of minimum temperature difference are distributed rather homogeneously over time across back-trajectories (not shown), i.e. there is not specific delay between the air mass crossing a convective system and the later observation of an SVC generated by the same air mass. The proportion of SVC with NAT-like optical properties (Sect. 5.1) stays the same (5–10 %) regardless if the air mass generating the cloud have interacted with convective activity or not.

Although these results cannot provide direct evidence to document how ice crystals nucleation led to SVC formation, they show that convective events appear in the recent history of 37 to 65 % of C1 SVC over Africa during JJA 2006.

## 6 Summary

In this study, we first documented on a global scale properties of optically thin layers identified in a previous paper as subvisible cirrus in more than 2 yr of CALIOP observations. Most of these layers are ∼ 500 m thick, colder than 195 K, extremely thin optically (optical depth below 0.015) and a few hundred kilometers wide. We documented the history of air masses that led to the formation of these SVC, using back-trajectories from the TRACZILLA model initialized at the location and time of SVC detection. Those air masses traveled equally over Asia, Central America and Africa. The mean latitude of their trajectories is near the equator in DJF while it is near 30° N in JJA (close to the AMA region). To restrict our analysis to SVC produced by air masses with a clearly





ACPD
12, 14875–14926, 2012



identifiable history, back-trajectories were classified based on their temperature history coherence over 5, 10 and 15 days. Most air masses leading to SVC with coherent temperature history observed in DJF Africa originate from Africa or nearby. In the JJA Pacific, more back-trajectories come from Central America and move west across the Pacific.

To investigate whether these layers should be seen as an extension of global population of high troposphere ice clouds towards thinner optical depths, or constitute a specific group with a different composition and formation processes, we studied the importance of three atmospheric phenomena in temperature-coherent back-trajectories over specific regions. Back-trajectories staying for more than 2 weeks in extreme TTL cold ($< 205$ K), coupled with the analysis of SVC optical properties through depolarization and color ratio, suggest heterogeneous nucleation involving uptake of non-ice species such as $HNO_3$ is a possible formation mechanism for a minority of SVC (3.4 %). Using spaceborne observations of $SO_2$ and $NO_2$ as proxies for the intensity of eruption and biomass burning events, we could not detect any short-term impact of local increase in the concentration of liquid and solid aerosols following said events on the SVC cloud cover. We could neither identify any instantaneous influence from enhanced stratospheric layers of sulfate-based aerosols created through direct injection of $SO_2$. We hinted at a possible correlation was found between an increase of tropical SVC cloud fraction (October to December 2006) and the dissipation of the low-stratosphere sulfate aerosol layer injected by the Soufriére Hills eruption. Finally, we studied when air masses leading to SVC formation previously intersected convective clouds identified by cold brightness temperatures in METEOSAT maps. We found 37 to 65 % of SVC are linked to air masses having recently interacted with convective activity (i.e. in the five days prior to cloud detection). This shows that SVC formation processes are very similar to other tropical ice clouds (e.g., Massie et al., 2002).

Our main objective in this paper was to establish if external processes could be a significant influence in the formation of the newly detected SVC population. By showing a strong link between SVC formation and convection, and a comparatively minor





ACPD
12, 14875–14926, 2012



influence of the two complementary processes studied ($HNO_3$ inclusion and local increases in liquid and hygroscopic aerosols), our results support the idea that the SVC population described in Martins et al. (2011) is to be first and foremost considered as an extension of the more general ice cloud population in the tropical UTLS towards thinner optical depths, and for a large part follow the same formation scenarios as optically thicker clouds.

Convection is the only mechanism that brings significant amounts of water vapor up in the TTL. It is thus expected that 100 % of water vapor leading to TTL cloud formation should eventually originate from a convective system, considering an infinite time scale. Sassen et al. (2009) and Riihimaki and McFarlane (2010) found 35 to 50 % of ice clouds in the tropical UTLS closely related to convection on near-instantaneous time scales. On the other side of the spectrum, Tzella and Legras (2011) followed air masses over 200 days and found that ∼80 % of them originate in a convective system, with an average ∼27 days to reach the 370 K potential temperature level from the surface, although vertical transport times have wide distributions. We consider a short time scale (5 days) and show that over this period almost 60 % of the air masses had potential interactions with convective events prior to cloud formation. Such results help to assess the significance of different formation hypotheses, e.g., Schwartz and Mace (2010).

Our results imply that the local increase of water vapor mixing ratio due to convection, or the advection of small ice crystals remaining after anvil precipitation, are significant formation scenarios for a large part of the SVC population. On the other hand, they also imply that at least 35 % of air masses leading to SVC formation had no recent interaction with convection, and were formed in situ through processes that still need to be identified as the two studied here have insufficient explanatory power. Which ice nuclei are statistically significant for SVC formation is unclear (Jensen et al., 2001), even if a large body of literature (e.g., Froyd et al., 2010) suggests the homogeneous nucleation of liquid sulfate-based aerosols play an important part. The present study could not adequately link instantaneous changes in SVC cloud fraction to local injections of





ACPD
12, 14875–14926, 2012



sulfate aerosols, in the troposphere or stratosphere, either from eruptions or convection. If these aerosols are indeed the primary source of ice nuclei in the UTLS, either (1) the amount of $SO_2$ loading created by the eruptions during the studied period is too small to have any significant impact; (2) the availability of water vapor, and not of ice nuclei, is limiting SVC formation or (3) another unidentified process inhibits water uptake on those aerosols.

In the near future, we plan to further investigate if the noticeable increase in tropical SVC cloud fraction in late 2006 can be traced back to the dissipation of the low-stratosphere aerosol layer from the Soufriére Hills. We also plan to combine the back-trajectory approach with case studies of SVC with specific optical properties, to better evaluate the nature of particles composing them, using for example in-situ measurements from the TC4 experiment (Toon et al., 2010). Another avenue of research we intend to explore involves identifying the point of SVC formation along the air mass trajectory. This would require access to the evolution of water vapor mixing ratio and supersaturation levels with time along the trajectory, which could be retrieved for instance from high-resolution water vapor fields out of mesoscale models and/or in-situ observations.

*Acknowledgements.* The authors would like to thank the IPSL computing and data centers ClimServ and CICLAD for computational facilities, the ICARE thematic center for data access, and the NASA Langley CALIPSO group for producing the CALIPSO data. Funding for part of this work was provided by the ANR project JC07_192911 and CNES.


The publication of this article is financed by CNRS-INSU.





ACPD
12, 14875–14926, 2012



## References


Arnaud, Y., Desbois, M., and Maizi, J.: Automatic tracking and characterization of African convective systems on meteosat pictures, J. Appl. Meteorol., 31, 443–453, 1992.

Bingemer, H., Klein, H., Ebert, M., Haunold, W., Bundke, U., Herrmann, T., Kandler, K., Müller-Ebert, D., Weinbruch, S., Judt, A., Wéber, A., Nillius, B., Ardon-Dryer, K., Levin, Z., and Curtius, J.: Atmospheric ice nuclei in the Eyjafjallajökull volcanic ash plume, Atmos. Chem. Phys., 12, 857–867, doi:10.5194/acp-12-857-2012, 2012.

Carn, S. A., Krotkov, N. A., Yang, K., Hoff, R. M., Prata, A. J., Krueger, A. J., Loughlin, S. C., and Levelt, P. F.: Extended observations of volcanic $SO_2$ and sulfate aerosol in the stratosphere, Atmos. Chem. Phys. Discuss., 7, 2857–2871, doi:10.5194/acpd-7-2857-2007, 2007.

Chepfer, H. and Noel, V.: A tropical "NAT-like" belt observed from space, Geophys. Res. Lett., 36, L03813, doi:10.1029/2008GL036289, 2009.

Chiriaco, M., Chepfer, H., Minnis, P., Haeffelin, M., Platnick, S., Baumgardner, D., Dubuisson, P., McGill, M., Noël, V., Pelon, J., Spangenberg, D., Sun-Mack, S., and Wind, G.: Comparison of CALIPSO-like, LaRC, and MODIS retrievals of ice-cloud properties over SIRTA in France and Florida during CRYSTAL-FACE, J. Appl. Meteorol. Clim., 46, 249–272, 2007.

Corti, T., Luo, B. P., de Reus, M., Brunner, D., Cairo, F., Mahoney, M. J., Martucci, G., Matthey, R., Mitev, V., dos Santos, F. H., Schiller, C., Shur, G., Sitnikov, N. M., Spelten, N., Vossing, H. J., Borrmann, S., and Peter, T.: Unprecedented evidence for deep convection hydrating the tropical stratosphere, Geophys. Res. Lett., 35, L10810, doi:10.1029/2008GL033641, 2008.

Davis, S. M., Avallone, L. M., Weinstock, E. M., Twohy, C. H., Smith, J. B., and Kok, G. L.: Comparisons of in situ measurements of cirrus cloud ice water content, J. Geophys. Res., 112, D10212, doi:10.1029/2006JD008214, 2007.

Davis, S., Hlavka, D., Jensen, E., Rosenlof, K., Yang, Q., Schmidt, S., Borrmann, S., Frey, W., Lawson, P., Voemel, H., and Bui, T. P.: In situ and lidar observations of tropopause subvisible cirrus clouds during TC4, J. Geophys. Res., 115, D00J17, doi:10.1029/2009JD013093, 2010.

Dee, D. P., Uppala, S. M., Simmons, A. J., Berrisford, P., Poli, P., Kobayashi, S., Andrae, U., Balmaseda, M. A., Balsamo, G., Bauer, P., Bechtold, P., Beljaars, A. C. M., van de Berg, L., Bidlot, J., Bormann, N., Delsol, C., Dragani, R., Fuentes, M., Geer, A. J., Haimberger, L., Healy, S. B., Hersbach, H., Hólm, E. V., Isaksen, L., Kållberg, P., Köhler, M., Matricardi, M.,






ACPD
12, 14875–14926, 2012



McNally, A. P., Monge-Sanz, B. M., Morcrette, J.-J., Park, B.-K., Peubey, C., de Rosnay, P., Tavolato, C., Thépaut, J.-N. and Vitart, F.: The ERA-interim reanalysis: configuration and performance of the data assimilation system, Q. J. Roy. Meteor. Soc., 137, 553–597, 2011.
Dupont, J.-C., Haeffelin, M., Morille, Y., Noel, V., Keckhut, P., Winker, D., Comstock, J. M., Chervet, P., and Robin, A.: Macrophysical and optical properties of midlatitude cirrus clouds from 4 ground-based lidars and collocated CALIOP observations, J. Geophys. Res., 115, D00H24, doi:10.1029/2009JD011943, 2010.
Froyd, K. D., Murphy, D. M., Lawson, P., Baumgardner, D., and Herman, R. L.: Aerosols that form subvisible cirrus at the tropical tropopause, Atmos. Chem. Phys., 10, 209–218, doi:10.5194/acp-10-209-2010, 2010.
Fueglistaler, S., Dessler, A. E., Dunkerton, T. J., Folkins, I., Fu, Q., and Mote, P. W.: Tropical tropopause layer, Rev. Geophys., 47, RG1004, doi:10.1029/2008RG000267, 2009.
Grenier, P. and Blanchet, J.-P.: Investigation of the sulphate-induced freezing inhibition effect from CloudSat and CALIPSO measurements, J. Geophys. Res., 115, D22205, doi:10.1029/2010JD013905, 2010.
Haladay, T. and Stephens, G.: Characteristics of tropical thin cirrus clouds deduced from joint CloudSat and CALIPSO observations, J. Geophys. Res., 114, D00A25, doi:10.1029/2008JD010675, 2009.
Heymsfield, A. J.: Ice particles observed in a cirriform cloud at −83 °C and implications for polar stratospheric clouds, J. Geophys. Sci., 43, 851–855, 1986.
James, R. and Legras, B.: Mixing processes and exchanges in the tropical and the subtropical UT/LS, Atmos. Chem. Phys., 9, 25–38, doi:10.5194/acp-9-25-2009, 2009.
Jensen, E. J., Toon., O. B., Pster, L., and Selkirk, H. B.: Dehydration of the upper troposphere and lower stratosphere by subvisible cirrus clouds near the tropical tropopause, Geophys. Res. Lett., 23, 825–828, 1996.
Jensen, E. J., Pfister, L., Ackerman, A., Tabazadeh, A., and Toon, O.: A conceptual model of the dehydration of air due to freeze-drying by optically thin, laminar cirrus rising slowly across the tropical tropopause, J. Geophys. Res., 106, 17237–17252, 2001.
Jensen, E. J., Pfister, L., Bui, T.-P., Lawson, P., and Baumgardner, D.: Ice nucleation and cloud microphysical properties in tropical tropopause layer cirrus, Atmos. Chem. Phys., 10, 1369–1384, doi:10.5194/acp-10-1369-2010, 2010.
Kärcher, B.: Properties of subvisible cirrus clouds formed by homogeneous freezing, Atmos. Chem. Phys., 2, 161–170, doi:10.5194/acp-2-161-2002, 2002.





ACPD
12, 14875–14926, 2012



Krämer, M., Schiller, C., Ziereis, H., Ovarlez, J., and Bunz, H.: Nitric acid partitioning in cirrus clouds: the role of aerosol particles and relative humidity, Tellus, 58, 141–147, 2006.
Krämer, M., Schiller, C., Afchine, A., Bauer, R., Gensch, I., Mangold, A., Schlicht, S., Spelten, N., Sitnikov, N., Borrmann, S., de Reus, M., and Spichtinger, P.: Ice supersaturations and cirrus cloud crystal numbers, Atmos. Chem. Phys., 9, 3505–3522, doi:10.5194/acp-9-3505-2009, 2009.
Lawson, R. P., Pilson, B., Baker, B., Mo, Q., Jensen, E., Pfister, L., and Bui, P.: Aircraft measurements of microphysical properties of subvisible cirrus in the tropical tropopause layer, Atmos. Chem. Phys., 8, 1609–1620, doi:10.5194/acp-8-1609-2008, 2008.
Lee, J., Yang, P., Dessler, A., Gao, B., and Platnick, S.: Distribution and radiative forcing of tropical thin cirrus clouds, J. Atmos. Sci., 66, 3721–3731, 2009.
Legras, B., Pisso, I., Berthet, G., and Lefèvre, F.: Variability of the Lagrangian turbulent diffusion in the lower stratosphere, Atmos. Chem. Phys., 5, 1605–1622, doi:10.5194/acp-5-1605-2005, 2005.
Lohmann, U., Karcher, B., and Timmreck, C.: Impact of the Mount Pinatubo eruption on cirrus clouds formed by homogeneous freezing in the ECHAM4 GCM, J. Geophys. Res., 108, 4568, doi:10.1029/2002JD003185, 2003.
Martins, E., Noel, V., and Chepfer, H.: Properties of cirrus and subvisible cirrus from nighttime Cloud-Aerosol Lidar Orthogonal Polarization (CALIOP), related to atmospheric dynamics and water vapor, J. Geophys. Res., 116, D02208, doi:10.1029/2010JD014519, 2011.
Massie, S., Gettelman, A., Randel, W., and Baumgardner, D.: Distribution of tropical cirrus in relation to convection, J. Geophys. Res., 107, 4591, doi:10.1029/2001JD001293, 2002.
Massie, S. T., Gille, J., Craig, C., Khosravi, R., Barnett, J., Read, W., and Winker, D.: HIRDLS and CALIPSO observations of tropical cirrus, J. Geophys. Res., 115, D00H11, doi:10.1029/2009JD012100, 2010.
McFarquhar, G. M., Heymsfield, A. J., Spinhirne, J., and Hart, B.: Thin and subvisual tropopause tropical cirrus: observations and radiative impacts, J. Atmos. Sci., 57, 1841–1853, 2000.
Murray, B. J.: Inhibition of ice crystallisation in highly viscous aqueous organic acid droplets, Atmos. Chem. Phys., 8, 5423–5433, doi:10.5194/acp-8-5423-2008, 2008.
Noel, V. and Chepfer, H.: Reply to comment by Poole et al. on "A tropical "NAT-like" belt observed from space", Geophys. Res. Lett., 36, L20804, doi:10.1029/2009GL039689, 2009.
Noel, V., Winker, D. M., Garrett, T. J., and McGill, M.: Extinction coefficients retrieved in deep tropical ice clouds from lidar observations using a CALIPSO-like algorithm compared to in-





ACPD
12, 14875–14926, 2012



situ measurements from the cloud integrating nephelometer during CRYSTAL-FACE, Atmos. Chem. Phys., 7, 1415–1422, doi:10.5194/acp-7-1415-2007, 2007.
Noel, V., Hertzog, A., Chepfer, H., and Winker, D.: Polar stratospheric clouds over Antarctica from the CALIPSO spaceborne lidar, J. Geophys. Res., 113, D0225, doi:10.1029/2007JD008616, 2008.
Pan, L. L. and Munchak, L. A.: Relationship of cloud top to the tropopause and jet structure from CALIPSO data, J. Geophys. Res., 116, D12201, doi:10.1029/2010JD015462, 2011.
Peter, Th., Luo, B. P., Wirth, M., Kiemle, C., Flentje, H., Yushkov, V. A., Khattatov, V., Rudakov, V., Thomas, A., Borrmann, S., Toci, G., Mazzinghi, P., Beuermann, J., Schiller, C., Cairo, F., Di Donfrancesco, G., Adriani, A., Volk, C. M., Strom, J., Noone, K., Mitev, V., MacKenzie, R. A., Carslaw, K. S., Trautmann, T., Santacesaria, V., and Stefanutti, L.: Ultrathin Tropical Tropopause Clouds (UTTCs): I. Cloud morphology and occurrence, Atmos. Chem. Phys., 3, 1083–1091, doi:10.5194/acp-3-1083-2003, 2003.
Peter, T., Marcolli, C., Spichtinger, P., Corti, T., Baker, M. B., and Koop, T.: When dry air is too humid, Science, 314, 1399–1402, 2006.
Petters, M. D., Carrico, C. M., Kreidenweis, S. M., Prenni, A. J., DeMott, P. J., Collett Jr., J. R., and Moosmüller, H.: Cloud condensation nucleation ability of biomass burning aerosol, J. Geophys. Res., 114, D22205, doi:10.1029/2009JD012353, 2009.
Pisso, I. and Legras, B.: Turbulent vertical diffusivity in the sub-tropical stratosphere, Atmos. Chem. Phys., 8, 697–707, doi:10.5194/acp-8-697-2008, 2008.
Platt, C. M. R., Young, S. A., Austin, R. T., Patterson, G. R., Mitchell, D. L., and Miller, S. D.: LIRAD observations of tropical cirrus clouds in MCTEX. Part I: Optical properties and detection of small particles in cold cirrus, J. Atmos. Sci., 59, 3145–3162., 2002.
Poole, L. R., Pitts, M. C., and Thomason, L. W.: Comment on "A tropical "NAT-like" belt observed from space" by Chepfer, H. and Noel, V., Geophys. Res. Lett., 36, L20803, doi:10.1029/2009GL038506, 2009.
Popp, P. J., Marcy, T. P., Jensen, E. J., Kärcher, B., Fahey, D. W., Gao, R. S., Thompson, T. L., Rosenlof, K. H., Richard, E. C., Herman, R. L., Weinstock, E. M., Smith, J. B., May, R. D., Vömel, H., Wilson, J. C., Heymsfield, A. J., Mahoney, M. J., and Thompson, A. M.: The observation of nitric acid-containing particles in the tropical lower stratosphere, Atmos. Chem. Phys., 6, 601–611, doi:10.5194/acp-6-601-2006, 2006.
Popp, P. J., Gao, R. S., Marcy, T. P., Fahey, D. W., Hudson, P. K., Thompson, T. L., Kärcher, B., Ridley, B. A., Weinheimer, A. J., Knapp, D. J., Montzka, D. D., Baumgardner, D. G., Gar-





ACPD
12, 14875–14926, 2012



rett, T. J., Weinstock, E. M., Smith, J. B., Sayres, D. S., Pittman, J. V., Dhaniyala, S., Bui, T. P., and Mahoney, M. J.: Nitric acid uptake on subtropical cirrus cloud particles, J. Geophys. Res., 109, D06302, doi:10.1029/2003JD004255, 2004.

Prata, A. J., Carn, S. A., Stohl, A., and Kerkmann, J.: Long range transport and fate of a stratospheric volcanic cloud from Soufrière Hills volcano, Montserrat, Atmos. Chem. Phys., 7, 5093–5103, doi:10.5194/acp-7-5093-2007, 2007.

Riihimaki, L. D. and McFarlane, S. A.: Frequency and morphology of tropical tropopause layer cirrus from CALIPSO observations: are isolated cirrus different from those connected to deep convection?, J. Geophys. Res., 115, D18201, doi:10.1029/2009JD013133, 2010.

Rossow, W. B. and Schiffer, R. A.: ISCCP cloud data products, B. Am. Meteorol. Soc., 72, 2–20, 1991.

Sassen, K.: The polarization lidar technique for cloud research: a review and current assessment, B. Am. Meteorol. Soc., 72, 1848–1866, 1991.

Sassen, K. and Benson, S.: A midlatitude cirrus cloud climatology from the facility for atmospheric remote sensing. Part II: Microphysical properties derived from lidar depolarisation, J. Atmos. Sci., 58, 2103–2112, 2001.

Sassen, K. and Cho, B. S.: Subvisual-thin cirrus lidar dataset for satellite verification and climatological research, J. Appl. Meteorol., 31, 1275–1285, 1992.

Sassen, K., Wang, Z., and Liu, D.: Global distribution of cirrus clouds from CloudSat/Cloud-Aerosol Lidar and Infrared Pathfinder Satellite Observations (CALIPSO) measurements, J. Geophys. Res., 113, D00A12, doi:10.1029/2008JD009972, 2008.

Sassen, K., Wang, Z., and Liu, D.: Cirrus clouds and deep convection in the tropics: insights from CALIPSO and CloudSat, J. Geophys. Res., 114, D00H06, doi:10.1029/2009JD011916, 2009.

Schwartz, M. C. and Mace, G. G.: Co-occurrence statistics of tropical tropopause layer cirrus with lower cloud layers as derived from CloudSat and CALIPSO data, J. Geophys. Res., 115, 20215, doi:10.1029/2009JD012778, 2010.

Sherwood, S., Minnis, P., McGill, M., and Chae, J.: Underestimation of deep convective clouds tops by thermal imagery, Geophys. Res. Lett., 31, L11102, doi:10.1029/2004GL019699, 2004.

Solomon, S., Rosenlof, K. H., Portmann, R. W., Daniel, J. S., Davis, S. M., Sanford, T. J., and Plattner, G.-K.: Contributions of stratospheric water vapor to decadal changes in the rate of global warming, Science, 327, 1219–1223, 2010.





ACPD
12, 14875–14926, 2012



Spichtinger, N., Wenig, M., James, P., Wagner, T., Platt, U., and Stohl, A.: Satellite detection of a continental-scale plume of nitrogen oxides from boreal forest fires, Geophys. Res. Lett., 28, 4579–4582, 2001.

Stohl, A., Forster, C., Frank, A., Seibert, P., and Wotawa, G.: Technical note: The Lagrangian particle dispersion model FLEXPART version 6.2, Atmos. Chem. Phys., 5, 2461–2474, doi:10.5194/acp-5-2461-2005, 2005.

Stubenrauch, C. J., Rossow, W. B., Cheruy, F., Chedin, A., and Scott, N. A.: Clouds as seen by satellite sounders (3I) and imagers (ISCCP). Part I: Evaluation of cloud parameters, J. Climate, 12, 2189–2213, 1999.

Thomas, A., Borrmann, S., Kiemle, C., Cairo, F., Volk, M., Beuermann, J., Lepuchov, B., Santacesaria, V., Matthey, R., Rudakov, V., Yushkov, V., Robert MacKenzie, A., and Stefanutti, L.: In situ measurements of background aerosol and subvisible cirrus in the tropical tropopause region, J. Geophys. Res., 107, 4763, doi:10.1029/2001JD001385, 2002.

Toon, O. B., Starr, D. O., Jensen, E. J., Newman, P. A., Platnick, S., Schoeberl, M. R., Wennberg, P. O., Wofsy, S. C., Kurylo, M. J., Maring, H., Jucks, K. W., Craig, M. S., Vasques, M. F., Pfister, L., Rosenlof, K. H., Selkirk, H. B., Colarco, P. R., Kawa, S. R., Mace, G. G., Minnis, P., and Pickering, K. E.: Planning, implementation, and first results of the Tropical Composition, Cloud and Climate Coupling Experiment (TC4), J. Geophys. Res., 115, D00J04, doi:10.1029/2009JD013073, 2010.

Tzella, A. and Legras, B.: A Lagrangian view of convective sources for transport of air across the Tropical Tropopause Layer: distribution, times and the radiative influence of clouds, Atmos. Chem. Phys., 11, 12517–12534, doi:10.5194/acp-11-12517-2011, 2011.

Vaughan, M. A., Liu, Z., McGill, M. J., Hu, Y., and Obland, M. D.: On the spectral dependence of backscatter from cirrus clouds: assessing CALIOP's 1064 nm calibration assumptions using cloud physics lidar measurements, J. Geophys. Res., 115, D14206, doi:10.1029/2009JD013086, 2010.

Vernier, J.-P., Thomason, L. W., Pommereau, J.-P., Bourassa, A., Pelon, J., Garnier, A., Hauchecorne, A., Blanot, L., Trepte, C., Degenstein, D., and Vargas, F.: Major influence of tropical volcanic eruptions on the stratospheric aerosol layer during the last decade, Geophys. Res. Let., 38, L12807, doi:10.1029/2011GL047563, 2011a.

Vernier, J.-P., Pommereau, J.-P., Thomason, L. W., Pelon, J., Garnier, A., Deshler, T., Jumelet, J., and Nielsen, J. K.: Overshooting of clean tropospheric air in the tropical





ACPD
12, 14875–14926, 2012



lower stratosphere as seen by the CALIPSO lidar, Atmos. Chem. Phys., 11, 9683–9696, doi:10.5194/acp-11-9683-2011, 2011.

Vernier, J.-P., Thomason, L. W., and Kar, J.: CALIPSO detection of an Asian tropopause aerosol layer, Geophys. Res. Lett., 38, L07804, doi:10.1029/2010GL046614, 2011c.

Voigt, C., Kärcher, B., Schlager, H., Schiller, C., Krämer, M., de Reus, M., Vössing, H., Borrmann, S., and Mitev, V.: In-situ observations and modeling of small nitric acid-containing ice crystals, Atmos. Chem. Phys., 7, 3373–3383, doi:10.5194/acp-7-3373-2007, 2007.

Voigt, C., Schlager, H., Roiger, A., Stenke, A., de Reus, M., Borrmann, S., Jensen, E., Schiller, C., Konopka, P., and Sitnikov, N.: Detection of reactive nitrogen containing particles in the tropopause region – evidence for a tropical nitric acid trihydrate (NAT) belt, Atmos. Chem. Phys., 8, 7421–7430, doi:10.5194/acp-8-7421-2008, 2008.

Wang, P.-H., McCormick, M. P., Poole, L. R., Chu, W. P., Yue, G. K., Kent, G. S., and Skeens, K. M.: Tropical high cloud characteristics derived from SAGE II extinction measurements, Atmos. Res., 34, 53–83, 1994.

Weigel, R., Borrmann, S., Kazil, J., Minikin, A., Stohl, A., Wilson, J. C., Reeves, J. M., Kunkel, D., de Reus, M., Frey, W., Lovejoy, E. R., Volk, C. M., Viciani, S., D'Amato, F., Schiller, C., Peter, T., Schlager, H., Cairo, F., Law, K. S., Shur, G. N., Belyaev, G. V., and Curtius, J.: In situ observations of new particle formation in the tropical upper troposphere: the role of clouds and the nucleation mechanism, Atmos. Chem. Phys., 11, 9983–10010, doi:10.5194/acp-11-9983-2011, 2011.

Winker, D.M, Vaughan, M. A., Omar, A., Hu, Y., and Powell, K. A.: Overview of the CALIPSO mission and CALIOP data processing algorithms, J. Atmos. Ocean. Tech., 26, 2310–2322, 2009.

Yang, K., Krotkov, N. A., Krueger, A. J., Carn, S. A., Bhartia, P. K., and Levelt, P. F.: Retrieval of large volcanic $SO_2$ columns from the aura ozone monitoring instrument: comparison and limitations, J. Geophys. Res., 112, D24S43, doi:10.1029/2007JD008825, 2007.

Yang, Q., Fu, Q., and Hu, Y.: Radiative impacts of clouds in the tropical tropopause layer, J. Geophys. Res., 115, D00H12, doi:10.1029/2009JD012393, 2010.





ACPD
12, 14875–14926, 2012



**Table 1.** Regions used in the study.

| Region | Latitude range | Longitude range |
|---|---|---|
| Asia | 30° S–20° N | 80° E–150° E |
| | 30° S–30° N | 150° E–180° E |
| Asian Monsoon Anticyclone (AMA) | 20° N–30° N | 50° W–150° E |
| Pacific | 30° S–30° N | 180° W–115° W |
| Central America | 30° S–30° N | 115° W–40° W |
| Africa | 30° S–30° N | 40° W–50° E |
| | 30° S–20° N | 50° E–80° E |





ACPD
12, 14875–14926, 2012



**Table 2.** Number of SVC according to their temperature history coherence in DJF and JJA (from 2006 to 2008) over 15 days back-trajectories.

| JJA | Africa | Asia | AMA | Central Am. | Pacific | Total |
|---|---|---|---|---|---|---|
| C1 | 117 | 61 | 24 | 71 | 59 | 332 (11.8 %) |
| C2 | 69 | 48 | 27 | 40 | 28 | 212 (7.5 %) |
| D | 590 | 891 | 198 | 307 | 280 | 2266 (80.6 %) |
| Total | 776 | 1000 | 249 | 418 | 367 | 2810 |
| | (27.6 %) | (35.6 %) | (8.9 %) | (14.9 %) | (13.1 %) | |
| DJF | Africa | Asia | AMA | Central Am. | Pacific | Total |
| C1 | 196 | 81 | 6 | 85 | 44 | 412 (10.2 %) |
| C2 | 108 | 80 | 2 | 40 | 36 | 266 (6.6 %) |
| D | 894 | 1305 | 32 | 579 | 551 | 3361 (83.2 %) |
| Total | 1198 | 1466 | 40 | 704 | 631 | 4039 |
| | (29.7 %) | (36.3 %) | (1 %) | (17.4 %) | (15.6 %) | |





ACPD
12, 14875–14926, 2012



**Table 3.** Number of C1 SVC with respect to temperature. Most SVC are located in 195–191 K.

| T (°K) | DJF | | | JJA | | | Total |
|---|---|---|---|---|---|---|---|
| | 2006–07 | 2007–08 | 2008–09 | 2006 | 2007 | 2008 | |
| 215–205 | 0 | 0 | 0 | 41 | 0 | 2 | 43 |
| 205–195 | 21 | 3 | 6 | 20 | 53 | 27 | 130 |
| 195–191 | 127 | 20 | 27 | 58 | 69 | 37 | 338 |
| 191–188 | 88 | 60 | 24 | 14 | 8 | 3 | 197 |
| 188–183 | 13 | 17 | 6 | 0 | 0 | 0 | 36 |
| Total | 249 | 100 | 63 | 133 | 130 | 69 | 744 |





ACPD
12, 14875–14926, 2012



**Table 4.** Statistics of average number of SVC for DJF and JJA over the different areas. Bold numbers indicate eruption periods.

| Area | Average Number of SVC | | | | | |
|---|---|---|---|---|---|---|
| | DJF67 | | | DJF78 | | |
| Pacific | 2.7 | 4.7 | 4.3 | 1.7 | 3.1 | 1.8 |
| Central America | 1.8 | 3.9 | 3.7 | 2.6 | 3.5 | 3.7 |
| Africa | **5.1** | **7.5** | **6** | 3.9 | 5.5 | 5 |
| Asia | **5.5** | **7.2** | **5.4** | 6.8 | 6.4 | 8.5 |
| AMA | **0.3** | **0.5** | **0.1** | 0 | 0.2 | 0.2 |

| Area | Average Number of SVC | | | | | | | | |
|---|---|---|---|---|---|---|---|---|---|
| | JJA6 | | | JJA7 | | | JJA8 | | |
| Pacific | **1** | **1.6** | **1.3** | 1.9 | 2.4 | 1.5 | 0.8 | 0.9 | 0.6 |
| Central America | 0.8 | 1.1 | 1.3 | 1.4 | 1.8 | 2.5 | 1.6 | 1.5 | 1.7 |
| Africa | 1.7 | 3.5 | 3.1 | 3.6 | 2.9 | 2.4 | 3 | 2.9 | 2.7 |
| Asia | **1.7** | **2.6** | **2.6** | 6.6 | 5.1 | 3.8 | 3.4 | 3.7 | 3.3 |
| AMA | 0.2 | 0.5 | 1 | 1.1 | 1.1 | 1.3 | 0.7 | 0.8 | 1.3 |





ACPD
12, 14875–14926, 2012



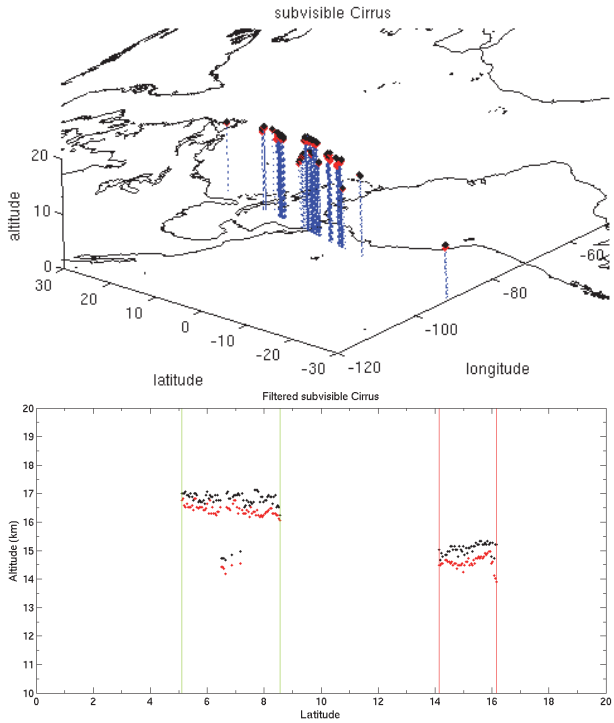


**Fig. 1.** (top) SVC detection along CALIPSO orbit on 6 August 2007 (orbit T07-03-58ZN). Vertical profiles are shown in blue, SVC detections appear in black (cloud top) and red (cloud base). (Bottom) Altitude of SVC clouds remain after layer filtering based on horizontal extent and temperature as a function of latitude.





ACPD
12, 14875–14926, 2012



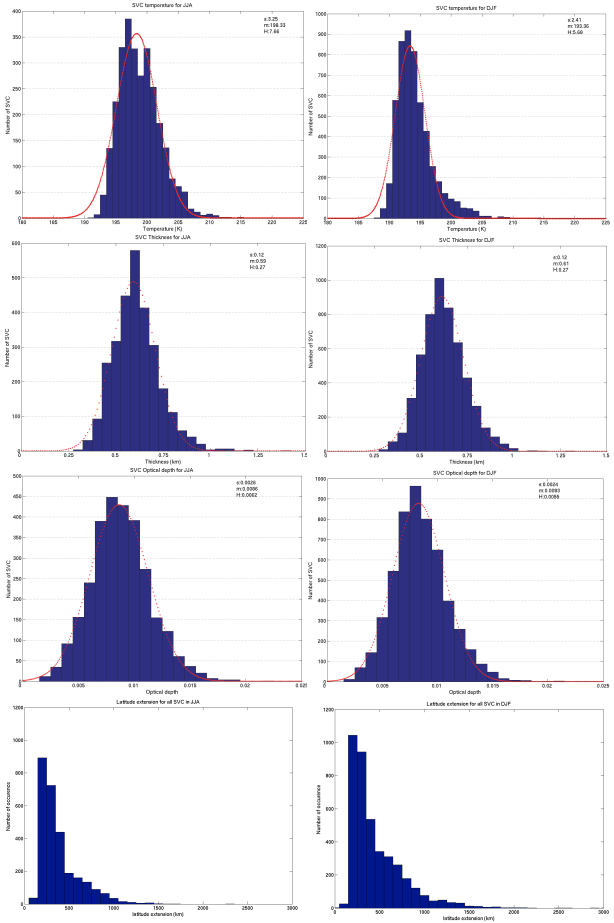

**Fig. 2.** Histograms of average temperature (row 1), geometrical (row 2) and optical thickness (row 3), and horizontal extension (row 4) for SVC in JJA (left column) and DJF (right), 2006–2008. The mean thickness of SVC is roughly equal to 600 m and the mean extension to 450 km.





ACPD
12, 14875–14926, 2012

On the origin of subvisible cirrus clouds in the tropical upper troposphere

M. Reverdy et al.



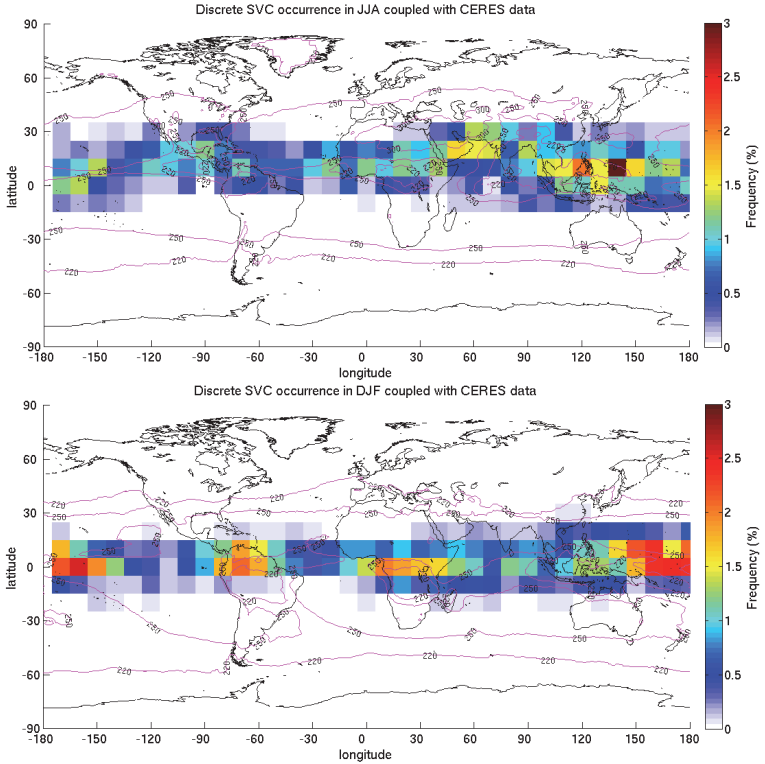


**Fig. 3.** Geographic distribution of SVC (in %) for JJA periods (top) and DJF (bottom) for 2006–2008. The sum of all boxes is 100 %. Contour lines show top of the atmosphere outgoing longwave flux (W m$^{-2}$) from CERES monthly means (EBAF product), averaged over the same periods.





ACPD
12, 14875–14926, 2012



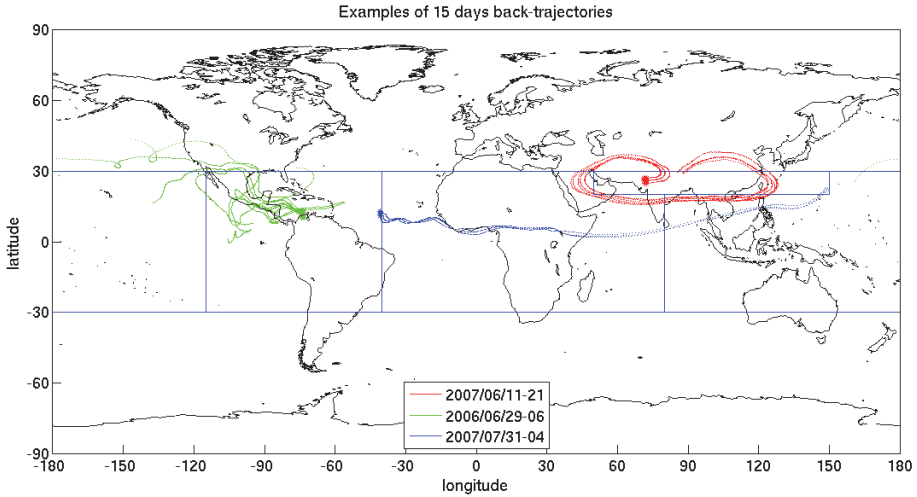


**Fig. 4.** Examples of three 15-days back-trajectories. For each, dots identify the position of the SVC used to initiate back-trajectory seeding.





ACPD
12, 14875–14926, 2012



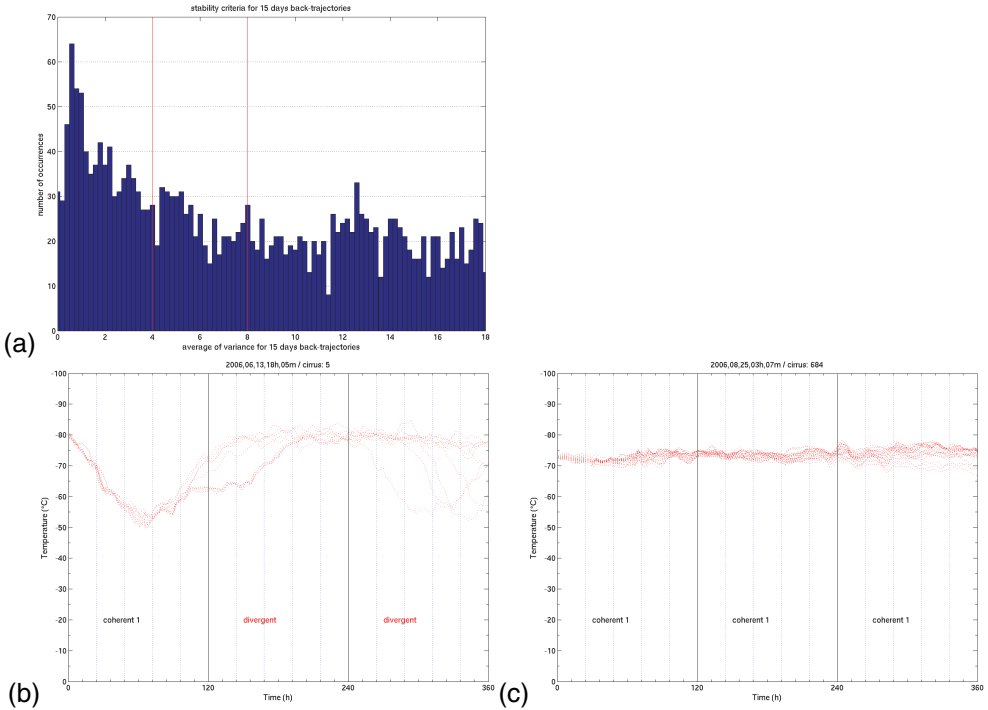


**Fig. 5. (a)** Histogram of temperature variance for 15 days back-trajectories for each SVC over 3 yr of data. Red lines represent the 3 different classifications. **(b, c)** Example of temperature histories across 15-days. The temperature coherence criteria is applied on 5 days periods.





ACPD
12, 14875–14926, 2012



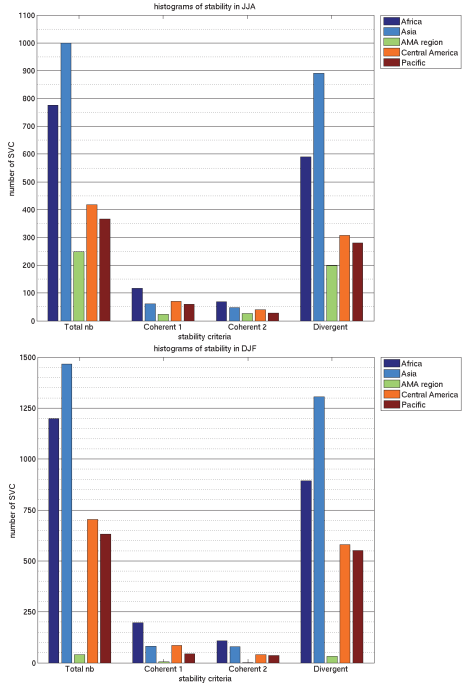


**Fig. 6.** Histograms of SVC temperature history coherence in JJA (top) and DJF (bottom) by area.





ACPD
12, 14875–14926, 2012



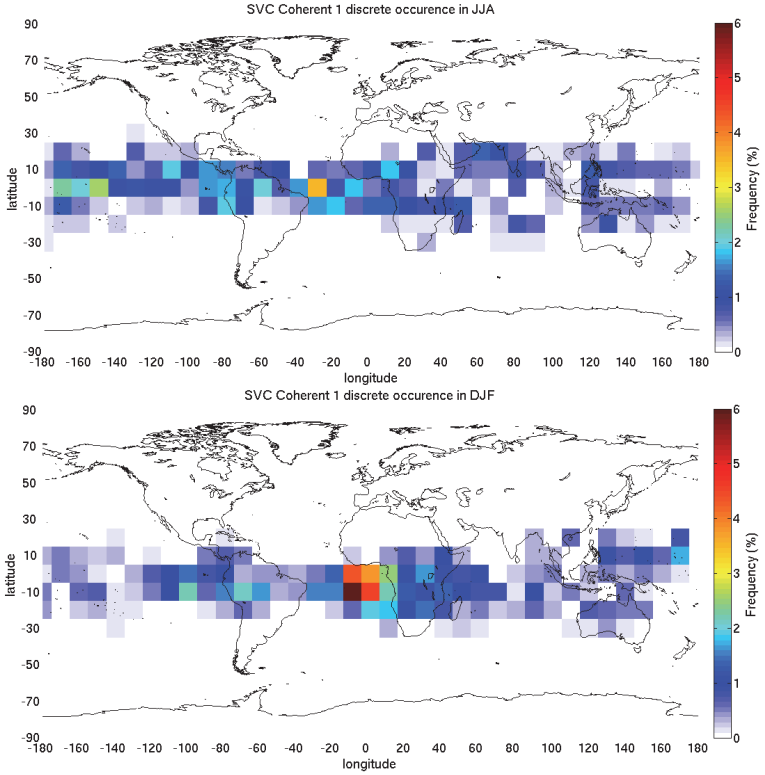


**Fig. 7.** Distribution of C1 SVC (% of total population) in JJA (top) and DJF (bottom).





ACPD
12, 14875–14926, 2012

On the origin of subvisible cirrus clouds in the tropical upper troposphere

M. Reverdy et al.



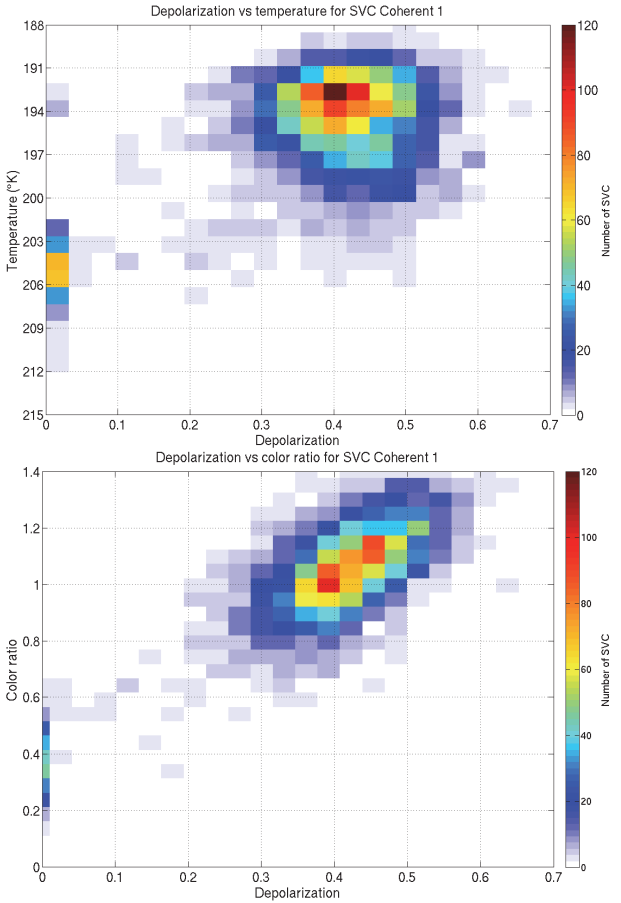


**Fig. 8.** Distributions of depolarization ratio vs. temperatures (top), and depolarization ratio vs. color ratio (bottom) for all C1 SVC over 15-days in 2006–2009.





ACPD
12, 14875–14926, 2012

On the origin of subvisible cirrus clouds in the tropical upper troposphere

M. Reverdy et al.



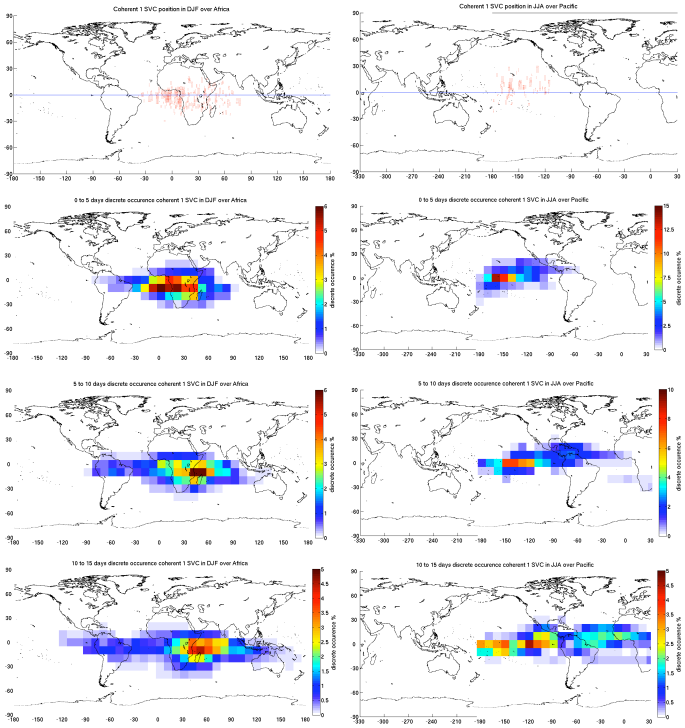

**Fig. 9.** Top: position of C1 SVC observed over Africa in DJF (left) and PaciLic in JJA (right). Second to fourth rows: spatial distribution of C1 back-trajectories over 0–5 days, 5–10 days, 10–15 days.





ACPD
12, 14875–14926, 2012

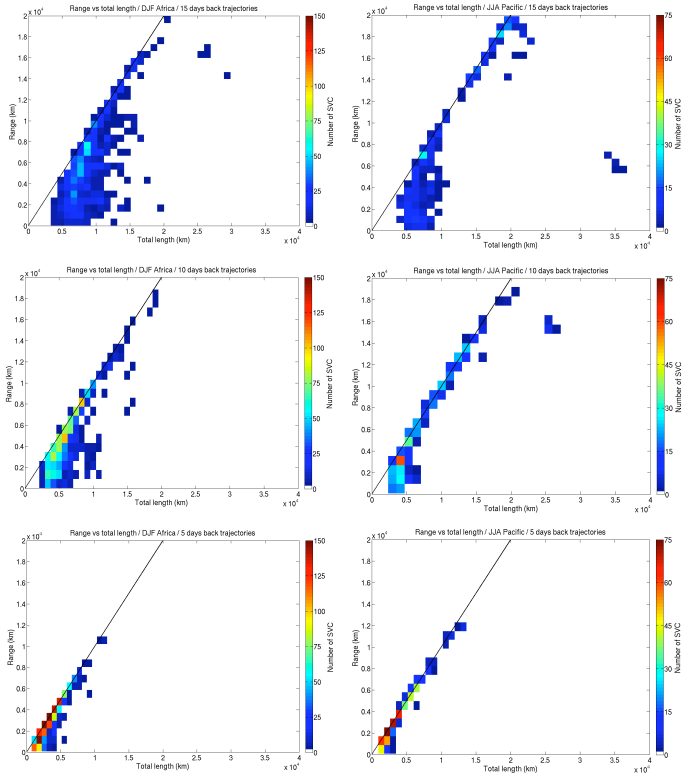


**Fig. 10.** Histograms of total back-trajectory length (horizontal) vs. reach away from the SVC (vertical) for 15-days (row 1),10-days (row 2) and 5-days (row 3) C1 back-trajectories over Africa in DJF (left) and over Pacific in JJA (right). The identity line is shown in black.





ACPD
12, 14875–14926, 2012

On the origin of subvisible cirrus clouds in the tropical upper troposphere

M. Reverdy et al.



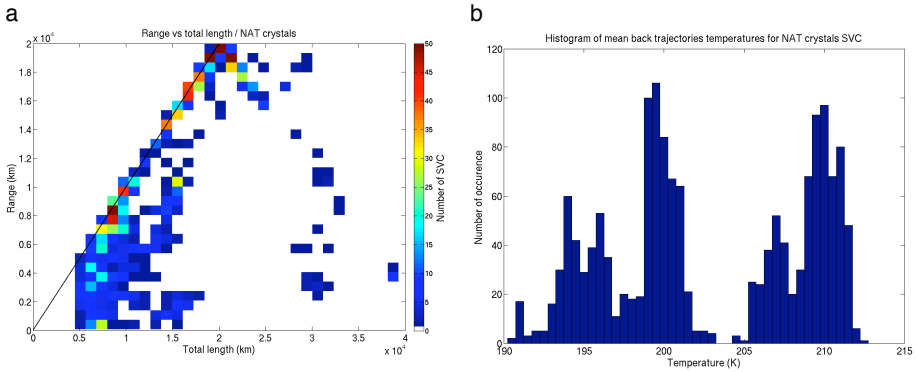


**Fig. 11.** Distribution of total trajectory length vs. reach away from the SVC (left column) and histograms of mean temperature along the back-trajectory (right column), for C1 SVC with depolarization ratios between 0.05 and 0.25.





ACPD
12, 14875–14926, 2012

On the origin of subvisible cirrus clouds in the tropical upper troposphere

M. Reverdy et al.



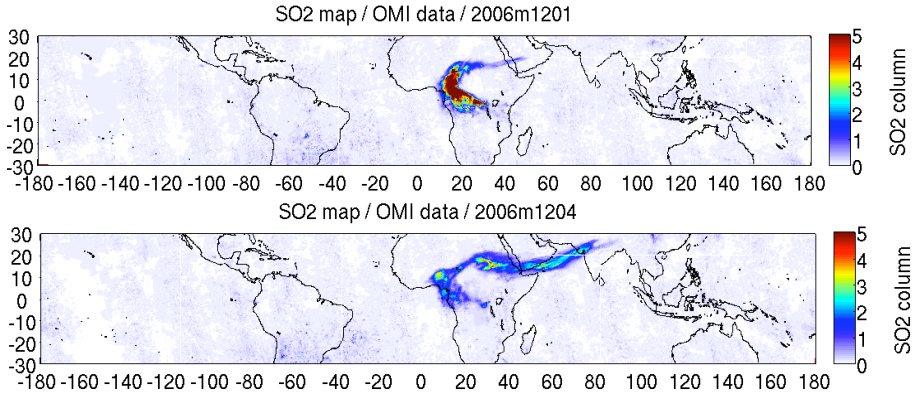


**Fig. 12.** Average column-integrated $SO_2$ concentrations (Dobson Units) on 27 November 2006 (top) and 1 December 2006 (bottom), near the eruption of Nyiragongo in DR Congo on late November, early December 2006.





ACPD
12, 14875–14926, 2012



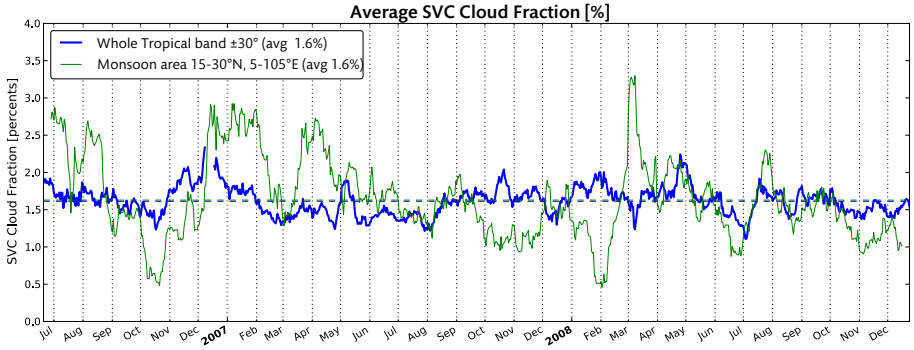


**Fig. 13.** Average cloud fraction of SVC (percents) in the tropical band (±30°, blue line) and the monsoon-affected area (green line, see text). CALIOP detections are smoothed out using a moving average over two-weeks for the tropical band, and over 1 month for the monsoon-affected area (a smaller sample size means noisier data). The almost overlapping horizontal dashed lines show the average for both time series.





ACPD
12, 14875–14926, 2012



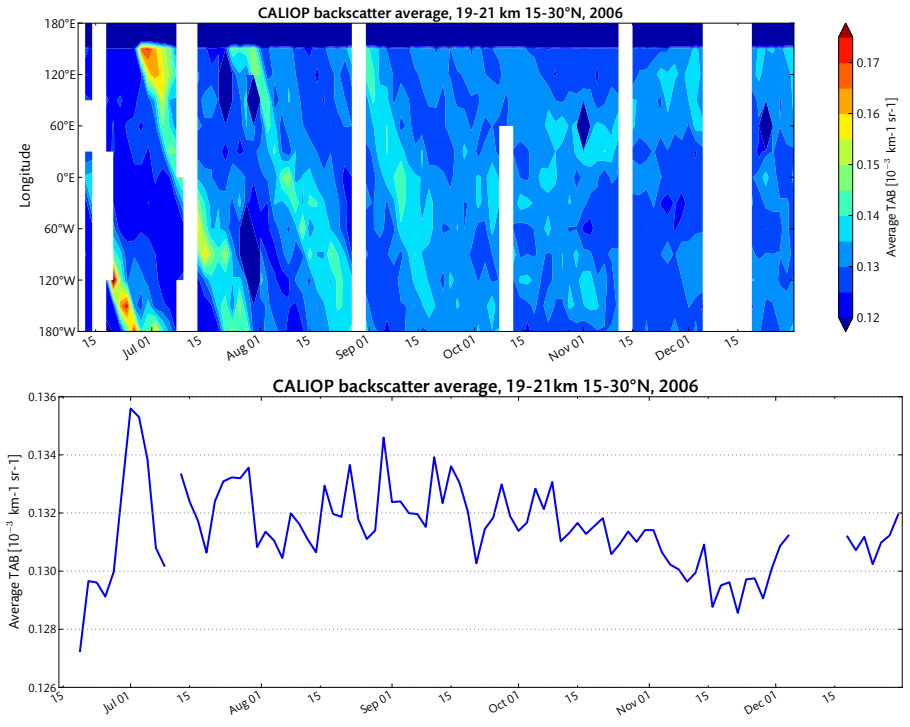


**Fig. 14.** Top: backscatter coefficient observed by CALIOP averaged between 19 and 21 km in the 15–30° N latitude band as a function of time (horizontal) and longitude (vertical) from June to December 2006. Bottom: same as above averaged on all longitudes.





ACPD
12, 14875–14926, 2012



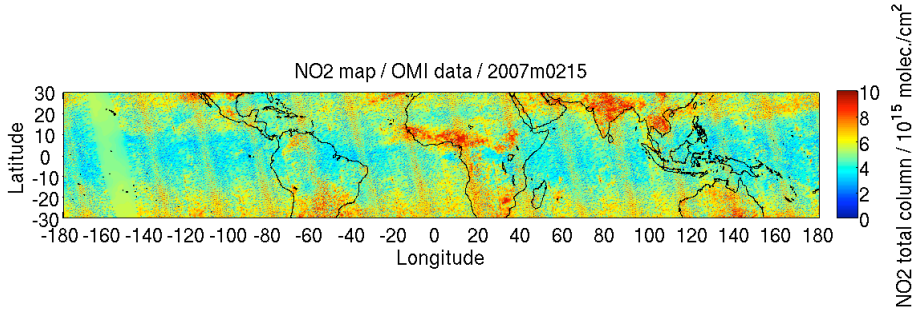


**Fig. 15.** Daily total column of $NO_2$ from OMI observations averaged over February 2007 and centered on Africa.





ACPD
12, 14875–14926, 2012



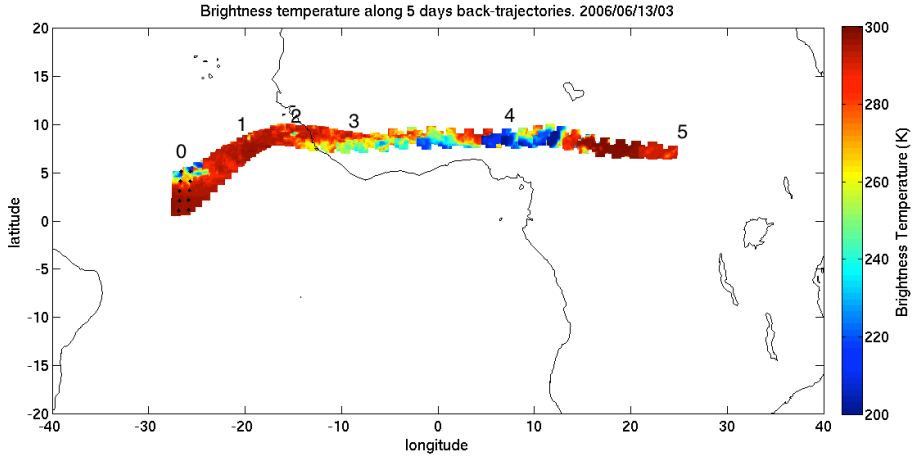


**Fig. 16.** Brightness temperatures (K) along 10 back-trajectories initialized on 13 June 2006 near 03:15 UTC (SVC detections near 27° E are marked by crosses). Days before SVC observation are numbered along the back-trajectories, showing that air masses slowed down significantly over the last 3 days. This composite map was produced by selecting for each back-trajectory point the ISCCP map closest in time, and extracting brightness temperatures 150 km around the point. 40 ISCCP maps were used.





ACPD
12, 14875–14926, 2012



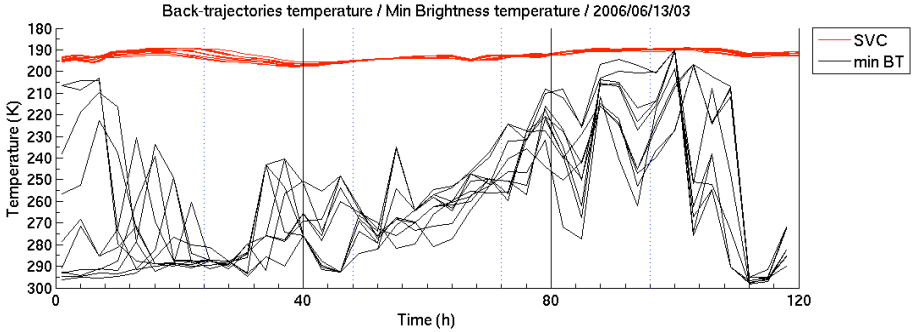


**Fig. 17.** Evolution of local temperature (red) and coldest brightness temperature from ISCCP (black) along the ten back-trajectories mapped in Fig. 15, as a function of time before SVC detection.





ACPD
12, 14875–14926, 2012



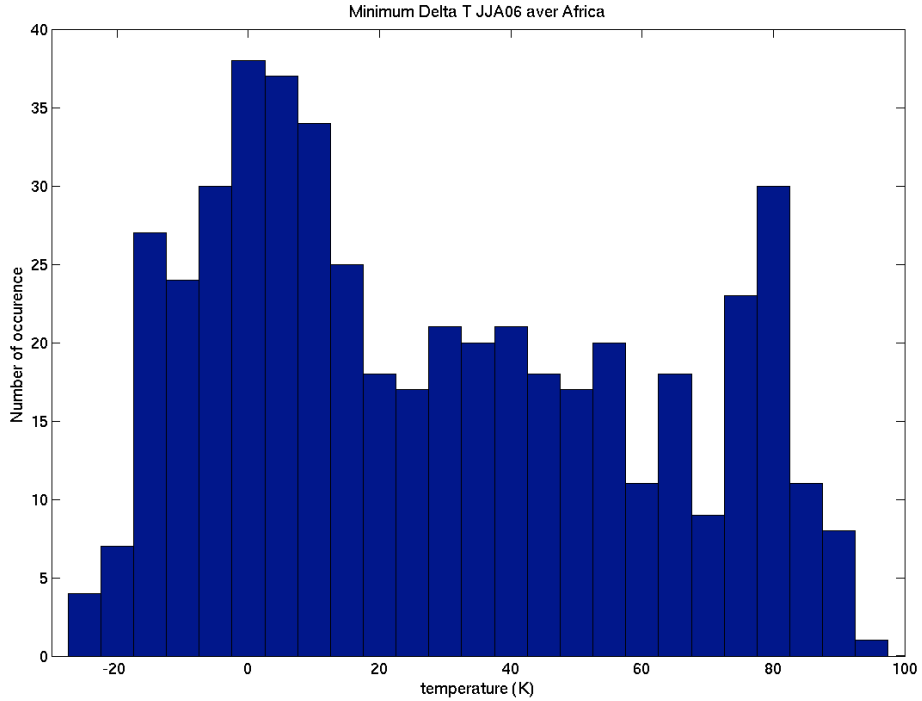


**Fig. 18.** Distribution of the smallest difference between the temperature at back-trajectory altitude and its surrounding brightness temperature for a given back-trajectory.





ACPD
12, 14875–14926, 2012